Nuclear Materials and Energy 48 (2026) 102171

Contents lists available at ScienceDirect

Nuclear Materials and Energy

journal homepage: www.elsevier.com/locate/nme

# Thermal cycling behaviour of $TiBe_{12}$ under fusion blanket relevant conditions

Ramil Gaisin [a,*], Sergey Udartsev [b], Maxim Kolmakov [b], Vladimir Chakin [a], Pavel Vladimirov [a], Francisco A. Hernández [a]

[a] Karlsruhe Institute of Technology, Kaiserstraße 12, 76131 Karlsruhe, Germany
[b] Ulba Metallurgical Plant, Abay Avenue 102, 070005 Ust-Kamenogorsk, Kazakhstan

ARTICLE INFO

*Keywords:*
Beryllides
Neutron multiplier material
Thermal cycling
Induction heating
DEMO

ABSTRACT

Titanium beryllide ($TiBe_{12}$) is a candidate neutron multiplier material for breeding blanket concepts in fusion reactors. In this study, thermal cycling experiments were performed on $TiBe_{12}$ blocks using induction heating and water cooling to investigate the response to transient thermal loading. Thermal cycling of a one-piece hexagonal $TiBe_{12}$ block resulted in fracture during the first heating cycle, attributed to non-uniform induction heating associated with the closed-loop block geometry. In contrast, a block subdivided into 12 $TiBe_{12}$ segments withstood 205 heating and cooling cycles between approximately 360 and 920°C without macroscopic cracking or fracture.

Additional experiments showed that $TiBe_{12}$ segments tolerate heating rates up to 1.1–1.3 K/s and cooling rates of about 1.2 K/s without failure. The results demonstrate that block segmentation significantly improves thermal cycling stability and provide experimental data for validation of thermo-mechanical models of beryllide blanket components under reactor-relevant transient conditions.

## Introduction

Within the helium-cooled pebble-bed (HCPB) breeding blanket concept developed for the DEMO fusion reactor, solid titanium beryllide ($TiBe_{12}$) blocks are considered as candidate neutron multiplier material [1]. Compared with conventional beryllium pebble beds, block-type $TiBe_{12}$ components offer advantages in terms of industrial-scale fabrication and structural integrity [2–4]. Furthermore, titanium beryllide exhibits lower chemical reactivity with air and steam, a higher melting temperature, high compressive strength maintained at elevated temperatures, a potentially higher allowable operating temperature, enhanced radiation resistance, and reduced tritium retention under neutron irradiation [5–11].

Intermetallic compounds are generally characterized by high hardness and limited ductility, which often results in brittle fracture behavior. This intrinsic material characteristic is of particular relevance for $TiBe_{12}$, as neutron multiplier blocks in pulsed fusion reactors are subjected to repetitive and rapid thermal transients. Such conditions may induce significant thermally generated stresses, promoting crack initiation and propagation in materials with low ductility and fracture toughness, as reported for titanium beryllide and other intermetallic systems [11–15]. To address these concerns, thermal cycling experiments on $TiBe_{12}$ blocks have been proposed to reproduce DEMO-relevant thermal loading conditions expected in fusion blanket applications. The present study pursues two primary objectives. The first objective is to investigate the influence of rapid heating and cooling, as well as the effect of block size and geometry, on crack formation and fracture behavior. The second objective is to experimentally validate the temperature distributions obtained from numerical simulations. This validation enables assessment of the thermophysical and thermo-mechanical material properties employed in the simulations and supports verification of the applied computational models and codes. In this work, the results of thermal cycling experiments performed on $TiBe_{12}$ blocks are presented. Particular emphasis is placed on in-situ temperature measurements, heating and cooling rates, and the evolution of material behavior during repeated thermal cycling.

## Materials and experimental techniques

The thermal cycling experiment was designed to reproduce the most critical thermal loading conditions expected for titanium beryllide neutron multiplier blocks in HCPB breeding blanket of the DEMO fusion

* Corresponding author.

https://doi.org/10.1016/j.nme.2026.102171
Received 26 March 2026; Received in revised form 28 May 2026; Accepted 15 June 2026
Available online 16 June 2026

reactor. According to the DEMO plasma pulse parameters, each pulse consists of ramp-up and ramp-down phases of 87.5 s and a full-power flat-top phase of 7200 s (Fig. 1) [16]. The first blanket modules are expected to operate for approximately 8000 plasma pulses over their service lifetime. This estimate is based on an assumed exposure of two full-power years and the DEMO pulse duration considered in this work. One pulse corresponds to approximately 2.22 h, resulting in about 8000 cycles for two full-power years of operation. While the quasi-stationary thermal conditions during the flat-top phase are not expected to be critical for $TiBe_{12}$, the rapid temperature changes occurring during the start-up and shutdown phases represent the most demanding thermal loading for this brittle intermetallic material. Thermal analyses of the HCPB blanket indicate that the most heavily loaded $TiBe_{12}$ blocks experience cyclic temperature variations in the range of approximately 370–920°C during reactor operation. To enable a clear comparison between reactor-relevant thermal loading and laboratory conditions, the temperature evolution of the most loaded block during a DEMO pulse was considered (Fig. 2a). For visualization purposes, the full-power flat-top duration was reduced to 600 s, allowing the heating and cooling transients to be resolved more clearly. The same figure also shows the simulated evolution of the peak temperature inside a $TiBe_{12}$ block for the thermal cycling experiment design described below. The thermal cycling profiles derived from the DEMO-relevant simulations resulted in cycle durations of approximately 8000 s when the full flat-top phase was retained. Such long cycles are impractical for laboratory testing; therefore, the flat-top duration was shortened while preserving the heating and cooling rates associated with the most critical phases of reactor operation. The resulting accelerated thermal cycle is shown in Fig. 2b and was used as the reference temperature–time profile for the experimental program.

The experimental concept is based on induction heating combined with internal water cooling. Induction heating was selected as the heating method because it allows rapid heating rates that are difficult to achieve in conventional resistance furnaces. In addition, induction heating provides more volumetric heat generation within electrically conductive materials due to eddy currents induced by the alternating magnetic field, which offers a qualitative similarity to the volumetric nuclear heating expected under neutron irradiation in DEMO. Water cooling was preferred over air or helium cooling owing to its higher heat transfer efficiency and the absence of pressurized gas loops, which simplifies the experimental setup.

According to the experimental design, hexagonal $TiBe_{12}$ blocks with a diameter of 144 mm and a height of 100 mm were selected for thermal cycling tests (Fig. 3). The block height was chosen primarily for ease of manufacture, as the HCPB blanket concept does not impose strict constraints on the axial length of individual neutron multiplier blocks [1]. The $TiBe_{12}$ blocks were manufactured at the Ulba Metallurgical Plant (UMP) using an industrial powder-based fabrication route developed previously for DEMO blanket applications [2]. The process is based on vacuum hot pressing of $TiBe_{12}$ powder, enabling the production of dense, large-scale blocks suitable for handling and testing. Two full-size hexagonal $TiBe_{12}$ blocks were fabricated using this technology and were employed in the present study (Fig. 4).

A dedicated thermal cycling facility was developed based on preliminary experiments and numerical simulations. A schematic view of the experimental concept is shown in Fig. 5. The $TiBe_{12}$ block was placed vertically inside a magnetic field generated by an induction coil. Cooling was provided by a stainless-steel pressure tube inserted into a central cylindrical channel machined in the block. The pressure tube had an outer diameter of 78 mm and was inserted into an 80 mm diameter hole, resulting in a 1 mm helium-filled annular gap between the tube and the block. This gap was introduced to compensate for the difference in thermal expansion between the $TiBe_{12}$ blocks and the stainless-steel pressure tube while maintaining mechanical decoupling, consistent with the gap concept employed in the HCPB blanket design of DEMO [1]. The stainless-steel pressure tube contained a central bore with a diameter of 35 mm for water cooling at a mass flow rate of 0.2 kg/s and a pressure of 1 bar (Fig. 6a,b).

To maintain sufficiently high water flow velocity and efficient heat transfer while limiting the total water consumption, a stainless-steel insert rod with a diameter of 25 mm was placed concentrically inside the tube (Fig. 6c,d). Stainless steel SS316L was selected as the pressure tube material due to its relatively low thermal conductivity compared with EUROFER97, which promotes higher surface temperatures of the tube and thereby facilitates the heating of the surrounding $TiBe_{12}$ block. Temperature monitoring was performed using five thermocouples

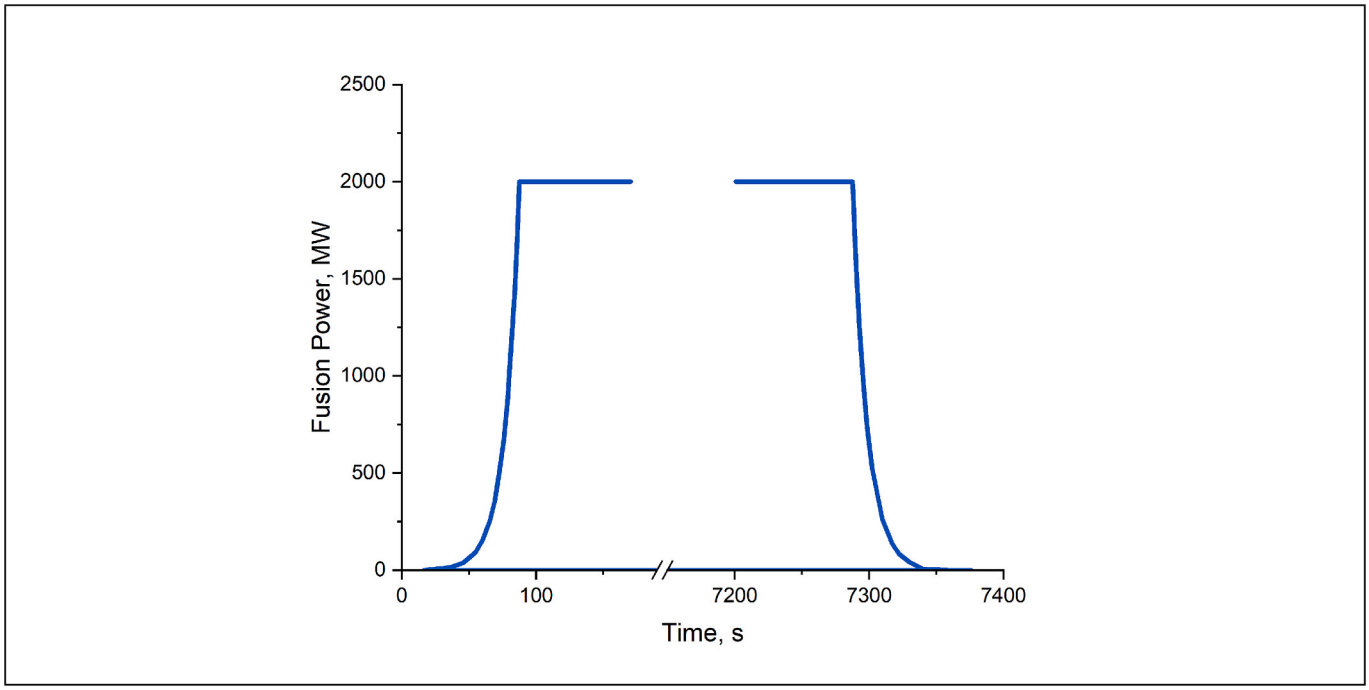


**Fig. 1.** The generated power of DEMO at the beginning and at the end of each pulse.

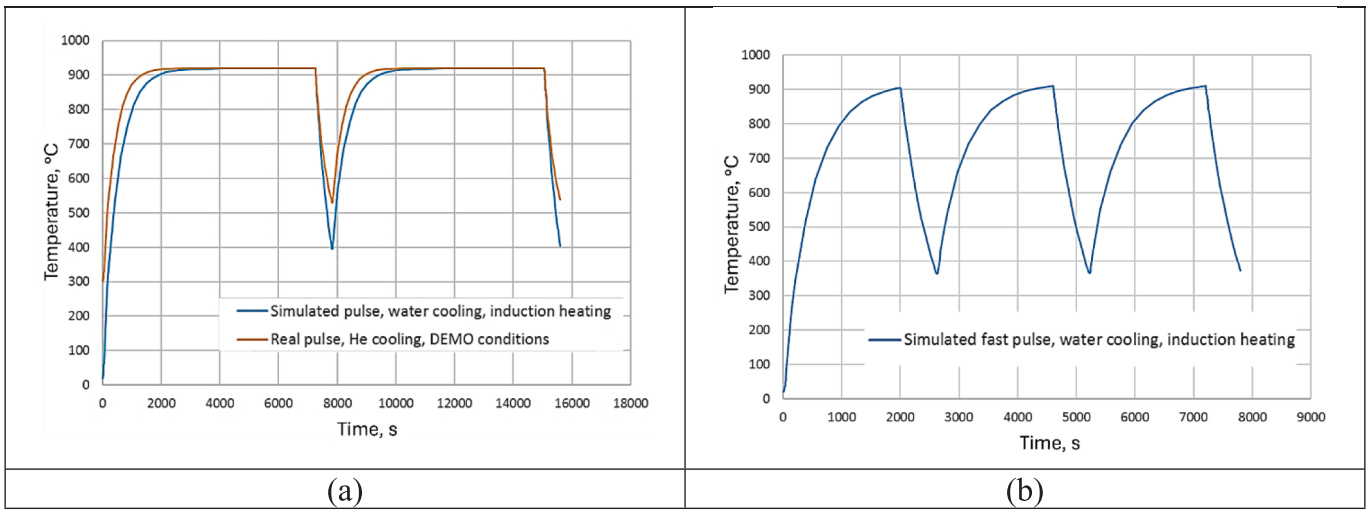


**Fig. 2.** (a) Maximum temperature evolution of the most loaded $TiBe_{12}$ block during plasma pulse in DEMO (orange), during simulated pulse using induction heating and water cooling (blue), and (b) during accelerated pulse using induction heating and water cooling with reduced heating time at maximum temperature. (For interpretation of the references to colour in this figure legend, the reader is referred to the web version of this article.)

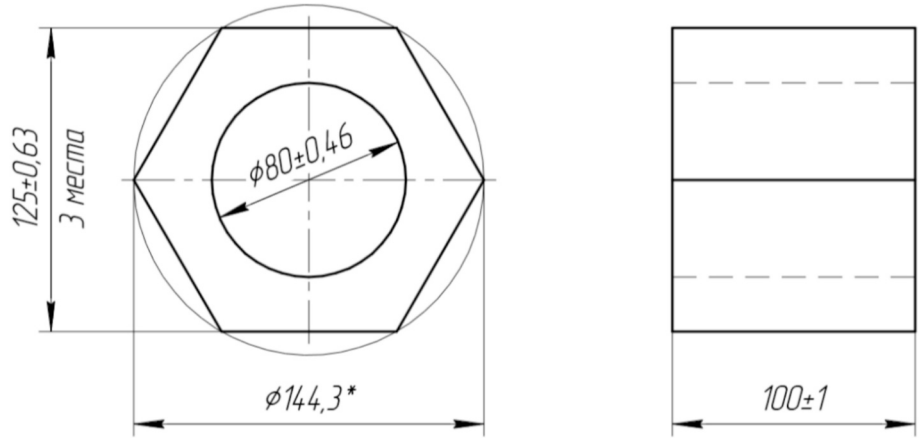


**Fig. 3.** Schematic drawing of the hexagonal $TiBe_{12}$ block used for the thermal cycling experiment.

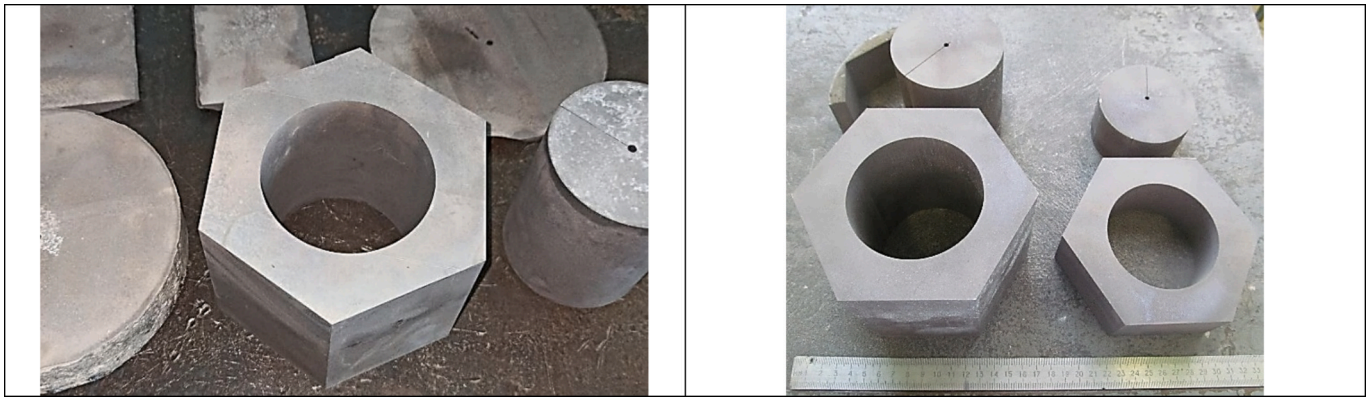

**Fig. 4.** Two full-size $TiBe_{12}$ blocks manufactured at the Ulba Metallurgical Plant and used in the thermal cycling experiments.

located on the outer edge and flat surface of the hexagonal block, on the inner surface of the central channel, on the outer surface of the pressure tube, and at the outlet of the cooling water. The upper surface of the block was covered with thermal insulation to reduce heat losses (Fig. 5).

The induction heating experiments were conducted at UMP, which possesses the necessary infrastructure and experience for manufacturing and handling $TiBe_{12}$ blocks. An industrial induction furnace operating at a frequency of 2400 Hz was employed.

The induction heating experiments were conducted at UMP, which possesses the necessary infrastructure and experience for manufacturing and handling $TiBe_{12}$ blocks. An industrial induction furnace operating at a frequency of 2400 Hz was employed. The electromagnetic penetration

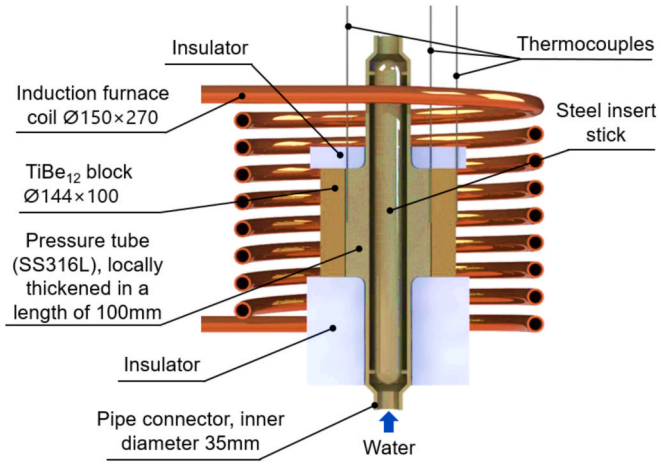


**Fig. 5.** Developed design of testing facility for thermal cycling of titanium beryllide.

depth was estimated using the classical skin-depth relation $\delta = (2/\omega\mu\sigma)^{1/2}$ [17], where $\omega = 2\pi f$, $\mu \approx \mu_0$ assuming non-ferromagnetic behavior of $TiBe_{12}$, and $\sigma$ is the electrical conductivity. Using the room-temperature electrical conductivity of $TiBe_{12}$, $\sigma = 5.1 \times 10^6$ S/m [2], the penetration depth at 2400 Hz is approximately 4.5 mm. Physically, this value corresponds to the characteristic depth at which the induced current density and electromagnetic field decrease by a factor of e compared with their surface values.

The furnace chamber, with an inner diameter of approximately 1200 mm, can be evacuated and backfilled with helium and is equipped with ports for water cooling, temperature measurements, and visual observation (Fig. 7a). The inner volume of the induction coil, approximately 400 mm in diameter and 270 mm in height, was sufficient to accommodate the thermal cycling assembly. The facility was assembled inside the furnace chamber, with magnesite used for the furnace hearth and corundum-based materials for the upper insulation (Fig. 7b,c). Thin layers of kaolin fabric were placed locally between the $TiBe_{12}$ block and the steel pressure tube to prevent unintended contact during thermal cycling. After assembly, the chamber was evacuated, purged several times with high-purity helium, and finally filled with helium to atmospheric pressure.

## Results and discussion

### *Thermal cycling of a one-piece hexagonal titanium beryllide block*

After completion of all preparatory steps and verification of water and helium tightness, the thermal cycling experiment of a one-piece hexagonal $TiBe_{12}$ block was initiated. At the initial stage, a trial heating procedure was performed in order to establish the relationship between the electrical parameters of the induction power supply and the temperatures measured at the selected control points. Prior to heating, the furnace chamber was evacuated to remove air, then purged several times with helium up to a pressure of approximately 0.3 bar, followed by repeated evacuation. Afterward, the chamber was filled with helium to a

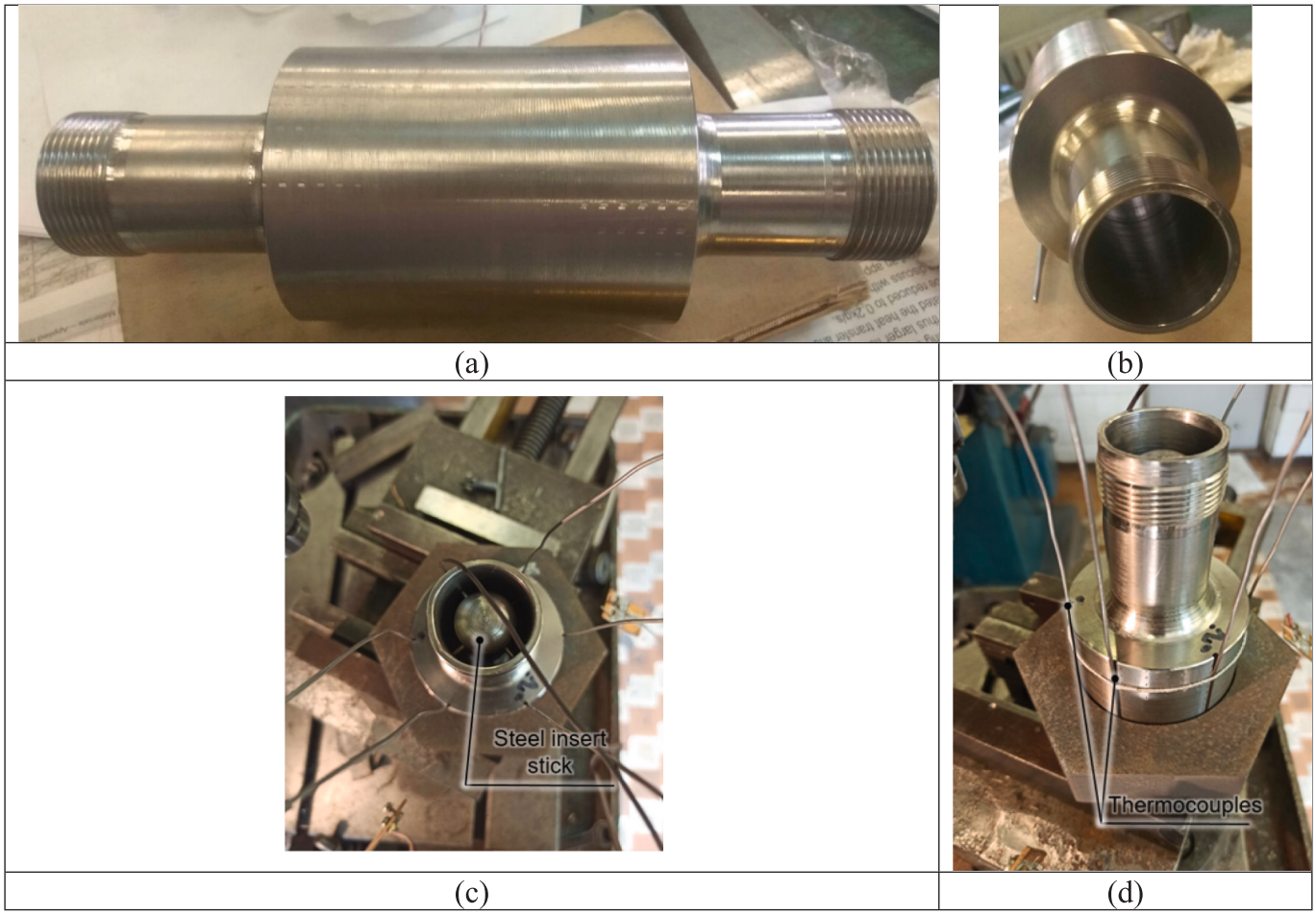


**Fig. 6.** Stainless steel pressure tube: (a) front view, (b) side view showing a 35 mm diameter hole, (c) side view showing an inserted steel stick, (e) pre-assembly with installation of thermocouples.

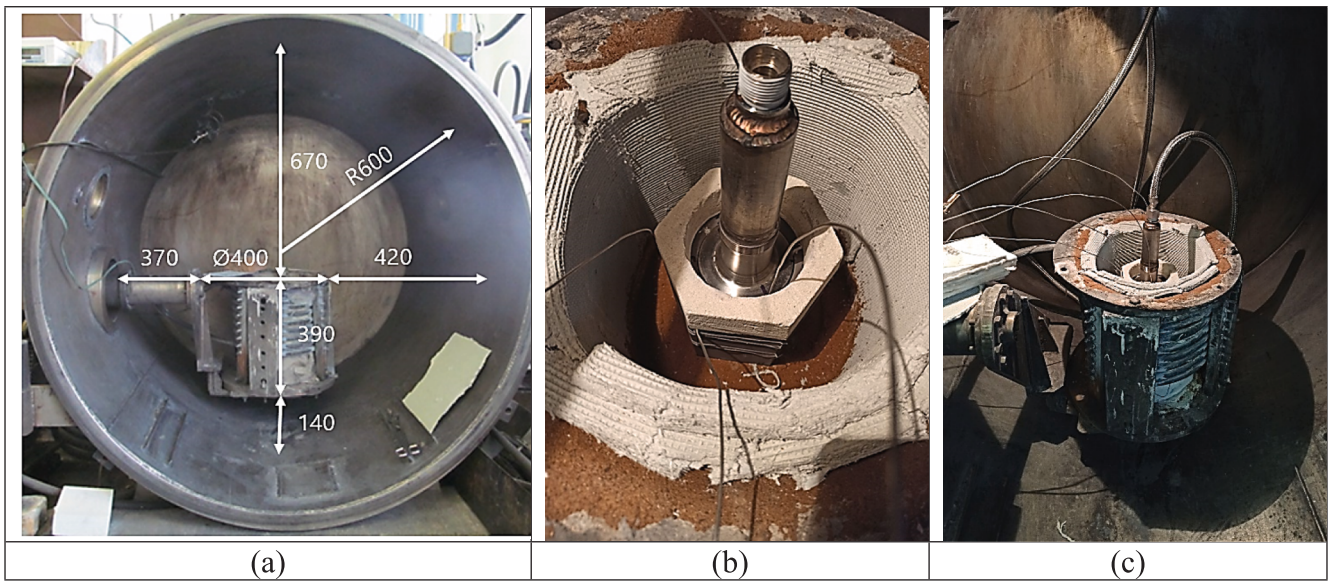


**Fig. 7.** Thermal cycling facility for $TiBe_{12}$ block testing: (a) induction furnace used for thermal cycling experiments;(b) $TiBe_{12}$ block installed with the stainless-steel pressure tube inside the induction furnace; (c) assembled thermal cycling setup before closing the chamber for evacuation and subsequent filling with helium.

pressure of 1 bar. The cooling water mass flow rate was set to 0.2 kg/s and was continuously monitored and adjusted during the experiment. During the initial heating stage, the block heated relatively slowly and in an apparently uniform manner. However, already during the first heating cycle, at a block temperature of approximately 400°C, a pronounced acoustic emission was detected, indicating the onset of cracking. Despite this observation, the heating was continued up to a maximum temperature of 800°C. No further acoustic events were recorded before reaching this temperature. Afterward, the system was allowed to cool down for subsequent inspection.

Fig. 8 presents the temperature evolution recorded by the thermocouples during the first heating cycle. At the minimum inductor power, the maximum temperature measured by thermocouple T1, corresponding to the outer edge surface of the block, was approximately 350°C. With successive discrete increases in inductor power, the temperatures on the block surface and on the stainless-steel pressure tube increased accordingly, reaching a maximum block surface temperature

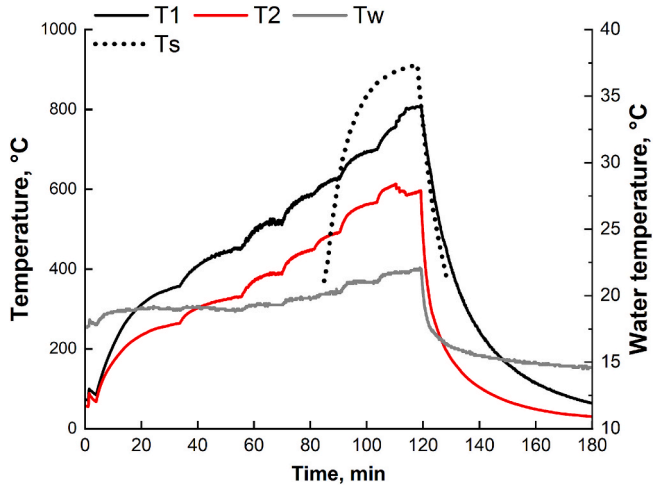


**Fig. 8.** Thermocouple readings during the first heating cycle of the titanium beryllide block: T1 — outer block surface at the edge; T2 — outer surface of the stainless-steel pressure tube; Tw — outlet water temperature; Ts — simulated temperature pulse with induction heating and water cooling and reduced dwell time at peak temperature (Fig. 2b).

of about 800°C. Induction heating of the block resulted in only minor heating of the cooling water, with the outlet temperature rising from approximately 15°C to 22°C. The average heating rate of the block outer surface was approximately 0.11 K/s, which is significantly lower than the maximum heating rate of about 0.8 K/s assumed in the simulated DEMO pulse (Fig. 2b). Short-term heating rates of up to 0.3 K/s were observed during stepwise changes of the inductor power. No distinct temperature anomalies were detected around 400°C, despite the audible cracking observed at this stage. The outer surface of the stainless-steel pressure tube heated more slowly than the $TiBe_{12}$ block; at a block surface temperature of 800°C, the temperature difference between the block surface and the tube surface was approximately 200°C, with the tube surface reaching a maximum temperature of about 600°C. After the inductor power was switched off, the block surface temperature decreased from 800°C to 350°C within approximately 780 s.

Post-test inspection of the block after opening the furnace chamber revealed that it had fractured into nine large fragments (Fig. 9). The block fractured predominantly along four radial cracks located in the thinnest region of the block wall. In addition, at least one crack extending approximately along the mid-height of the block was observed on the lateral surfaces (Fig. 9c). The fracture surfaces appeared clean and did not show visible defects such as porosity or foreign inclusions (Fig. 9d).

Based on the observed fracture pattern and the thermal history of the experiment, several possible causes of the block failure were initially considered. These included excessive thermal stresses generated during heating, intrinsic brittleness of the material, and the influence of block geometry on the induction heating conditions. However, no macroscopic defects, porosity, or foreign inclusions were detected on the fracture surfaces, which appeared clean and characteristic of brittle failure. Moreover, previous thermal cycling experiments performed on smaller $TiBe_{12}$ specimens as well as on more massive components manufactured using the same production route did not result in crack formation. This indicates that neither the intrinsic brittleness of the material nor the applied heating rates alone are sufficient to explain the observed fracture of the one-piece hexagonal block. Consequently, the dominant factor was attributed to the specific geometry of the block under induction heating. Owing to its closed-loop configuration, strong eddy currents are induced along the outer perimeter of the solid block, resulting in pronounced surface-localized heating. In contrast, the central regions of the block are heated predominantly by thermal

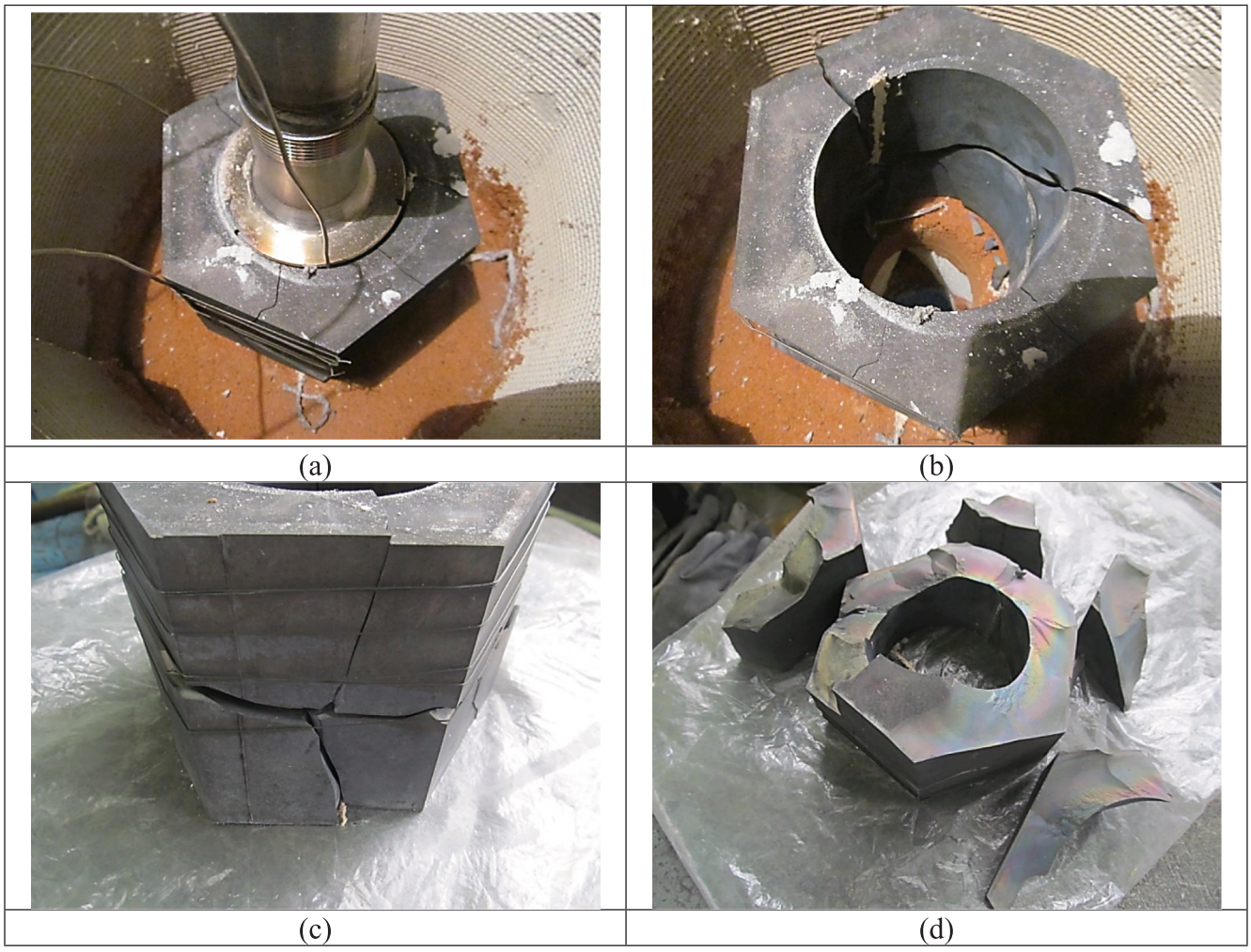


**Fig. 9.** $TiBe_{12}$ block after a single heating and cooling cycle: (a) after opening the furnace chamber, (b) after removal of the pressure tube, (c) lateral surface cracks, (d) separated block fragments.

conduction. This leads to steep radial temperature gradients and, consequently, to large thermal stresses arising from differential thermal expansion between the rapidly heated outer surface and the cooler interior. These stresses are considered to exceed the fracture strength of $TiBe_{12}$, leading to crack initiation and propagation during the first heating cycle.

To further assess the role of geometry and current distribution, a follow-up experiment was performed using the fractured block itself. The nine large fragments formed after the initial failure were reassembled and mechanically fixed using a nickel–chromium wire, forming a discontinuous block assembly. The reassembled block was then subjected to two additional heating and cooling cycles in the same induction heating setup (Fig. 10a).

Post-test inspection revealed that no further fragmentation of the block occurred during these additional cycles (Fig. 10b-d). However, localized bright spots were observed on the lateral surfaces at the contact regions between individual fragments. These features are attributed to electrical sparking caused by induced currents flowing along the outer circuit of the assembled block, leading to localized overheating and minor surface damage.

Taken together, these results suggest that the fracture of the original one-piece hexagonal $TiBe_{12}$ block is most likely associated with its closed-loop geometry under induction heating, rather than with an intrinsic limitation of the material itself. Under such conditions, eddy currents are expected to be concentrated along the outer perimeter of the block, potentially leading to strongly non-uniform surface heating and the development of high thermal stresses. In contrast, under the operating conditions of the DEMO HCPB blanket, heating is expected to occur volumetrically due to neutron irradiation, resulting in a significantly more uniform temperature distribution within the material. On this basis, it was hypothesized that thermal cycling of a solid $TiBe_{12}$ block in an induction furnace may not adequately reproduce the thermal loading conditions expected in a fusion reactor blanket. This consideration motivated a modification of the experimental approach and the development of an alternative block configuration for subsequent thermal cycling experiments.

It should be emphasized that induction heating was selected as a compromise approach capable of reproducing rapid thermal transients under controlled helium atmosphere conditions. Conventional resistance heating would provide substantially slower heating rate and would therefore not allow reproduction of DEMO-relevant transient conditions. Alternative approaches, such as electron-beam heating, would introduce excessive local power densities and are difficult to implement in a closed helium-filled chamber with integrated internal cooling. For this reason, induction heating combined with water cooling was considered the most practical experimental solution for the present study.

Nevertheless, the experiments revealed important limitations of this approach. In order to achieve sufficiently rapid heating rates, relatively high induction power had to be applied. Under such conditions, heat generation becomes strongly localized near the outer surface of the $TiBe_{12}$ block due to eddy current concentration and limited

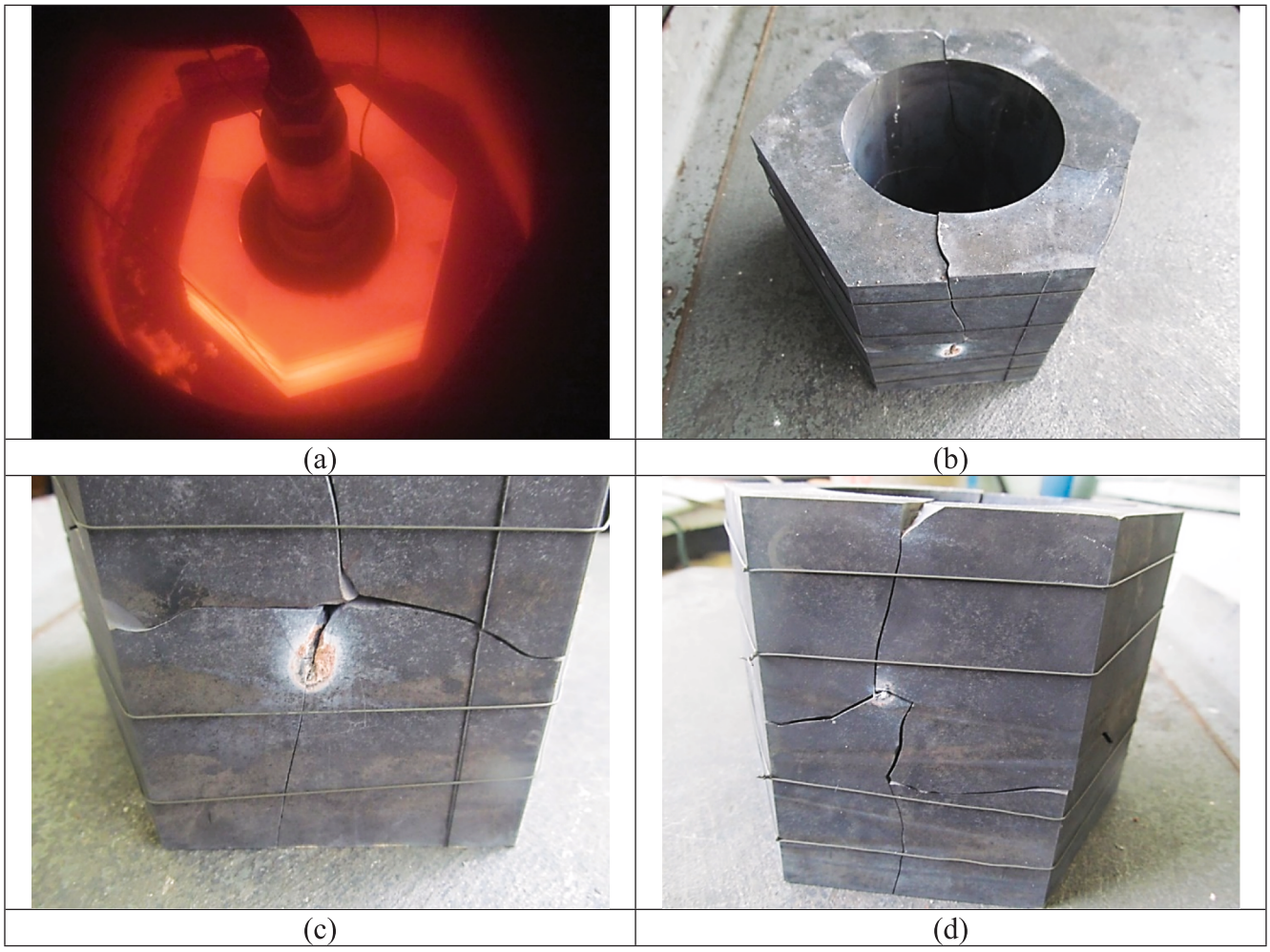


**Fig. 10.** Fractured $TiBe_{12}$ block during and after repeated thermal cycling: (a) inside the induction furnace, (b–d) surface appearance after two additional cycles.

electromagnetic penetration depth. According to conservative estimates, the effective penetration depth under the applied experimental conditions is limited to only several millimeters ($\delta \approx 4.5$ mm), whereas the minimum wall thickness of the one-piece block is 22.5 mm. As a consequence, the outer regions of the block experience rapid ohmic heating, while the central part is heated predominantly by thermal conduction, leading to the formation of too large radial temperature gradients and correspondingly high thermal stresses.

Under actual DEMO blanket conditions, neutron heating is expected to occur volumetrically throughout the neutron multiplier block, although some temperature gradient will still exist due to neutron attenuation and the gradual reduction of nuclear heating from the first-wall side toward the backplate of the blanket. However, these gradients are expected to be substantially smaller than those generated under induction heating conditions. Therefore, the present induction heating experiments may be regarded as a conservative thermal loading scenario. If $TiBe_{12}$ blocks are capable of withstanding such severe surface-localized heating without fracture, their behavior under more homogeneous volumetric neutron heating is expected to be more favorable. At the same time, the fracture of the one-piece $TiBe_{12}$ block demonstrates that such conservative thermal loading conditions cannot be tolerated by a solid closed-loop geometry. This observation motivated the modification of the experimental concept and the development of the segmented block configuration investigated in the subsequent experiments.

*Thermal cycling of a segmented hexagonal $TiBe_{12}$ block*

Based on the hypothesis that the fracture of the one-piece hexagonal $TiBe_{12}$ block was associated with its closed-loop geometry under induction heating, an alternative experimental approach was proposed. The main objective was to achieve a more uniform temperature distribution within the block and to reduce thermally induced stresses by subdividing the material into several electrically and thermally independent segments. Such segmentation promotes more homogeneous induction heating by creating multiple independent current paths and simultaneously reduces thermal stresses during heating and cooling by limiting the characteristic dimensions over which thermal expansion mismatch can develop.

Fig. 11a illustrates an alternative design concept for titanium beryllide blocks without a central hole, in which the space between steel cooling tubes can be filled with blocks of more complex shapes. Such blocks are simpler and more cost-effective to manufacture, as drilling of a central channel is not required. However, direct thermal cycling of complex-shaped blocks in an induction furnace is challenging, since each cylindrical surface would require individual cooling, and the presence of multiple steel tubes would significantly shield the magnetic field and interfere with induction heating.

To overcome these limitations while preserving the essential geometric features of the alternative block concept, a segmentation strategy was adopted. Each complex-shaped block was conceptually divided into three identical parts, and a hexagonal block was assembled from six such segments. Fig. 11b shows the proposed sectioning scheme applied to the

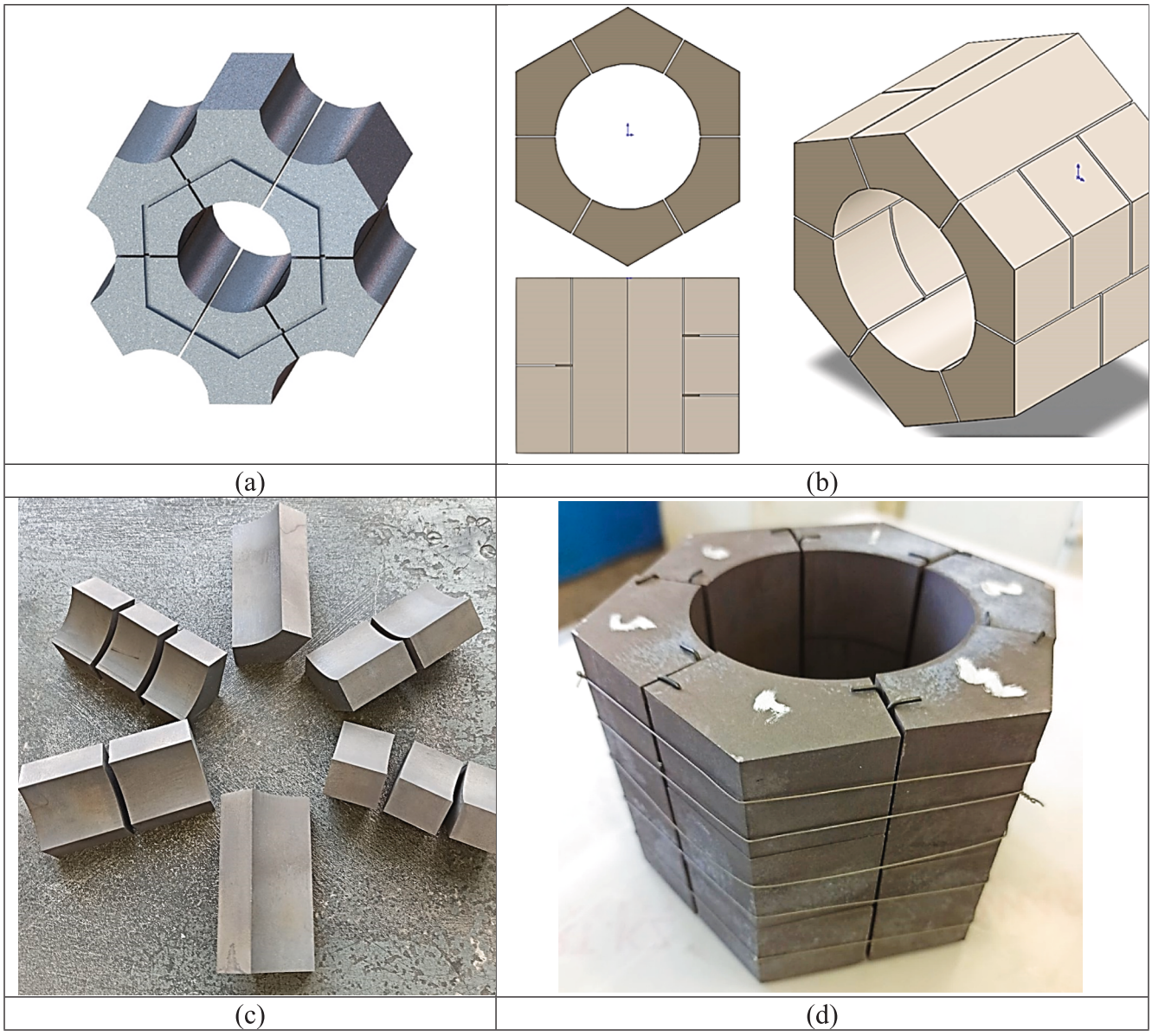


**Fig. 11.** Segmentation concept for thermal cycling of titanium beryllide blocks: (a) alternative design of $TiBe_{12}$ blocks of complex shape without a central hole, (b) proposed cutting scheme of a hexagonal block to simulate thermal cycling of blocks with alternative geometry, (c) block segments after cutting into 12 pieces, (d) hexagonal block assembled from 12 $TiBe_{12}$ segments.

second manufactured hexagonal $TiBe_{12}$ block. The block was first cut into six segments along the thinnest region of the wall. Since, in addition to radial cracks, at least one crack had previously been observed near the mid-height of the block (Fig. 9), further subdivision along the height was introduced to investigate the influence of segment height on crack formation. Specifically, two of the six segments were divided into two pieces with a height of 50 mm, two segments were divided into three pieces with a height of 33 mm, and the remaining two segments were kept at the original height of 100 mm. As a result, a composed block consisting of 12 individual $TiBe_{12}$ segments was obtained (Fig. 11c,d). To maintain a small gap between adjacent segments and to prevent direct electrical contact and sparking, rods with a diameter of 1.5 mm made of beryllium bronze (BrB2) were inserted between the segments (Fig. 11d).

After installation of the composed block into the thermal cycling facility, an initial heating test was performed. Unlike the initial experiment with the one-piece block, where cautious heating conditions were applied during the first trial cycle, the heating parameters for the segmented configuration were subsequently adjusted in order to approach the simulated DEMO transient conditions more closely. At the maximum available inductor power, the block reached a temperature of approximately 840°C after 35 min. Subsequent visual inspection revealed that all segments retained their integrity (Fig. 12a). It was assumed that the maximum attainable temperature was limited by increased heat losses from the outer surface of the segmented block. To reduce these losses, the lateral surface of the block was covered with an additional 7 mm thick thermal insulation layer (Fig. 12b). Following this modification, the required target temperatures were successfully achieved during heating (Fig. 12c).

The thermal cycling experiment was conducted continuously over a total period of 26 days. A minimum of 200 cycles was selected in order to complete the experimental campaign within a reasonable timeframe. During operation, the segmented block was visually monitored through the furnace window. Periodically, the chamber was opened and the block was inspected either in assembled form or after partial or complete disassembly. Due to increased helium diffusion at elevated

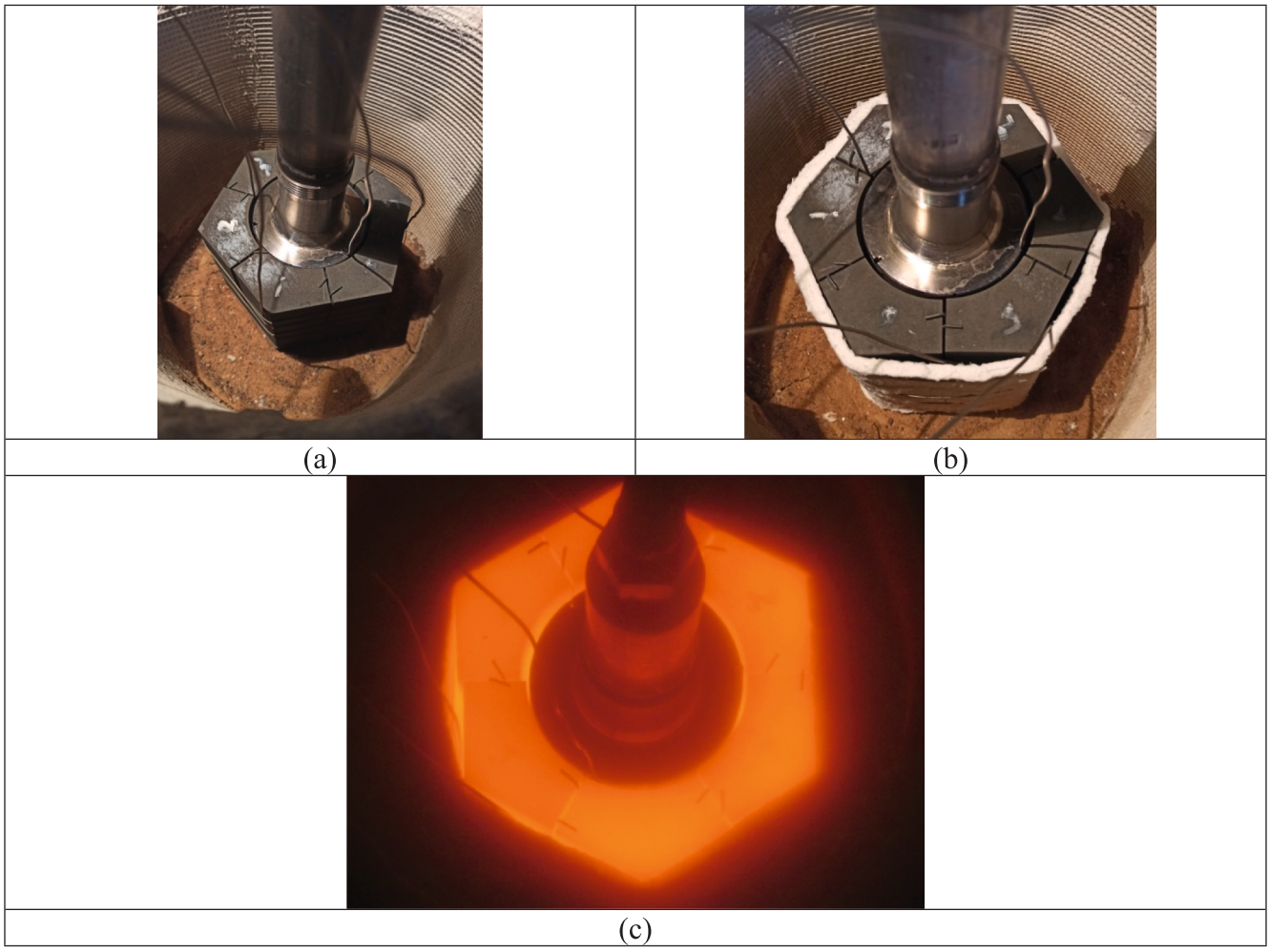


**Fig. 12.** Thermal cycling of the segmented $TiBe_{12}$ block: (a) assembled block after the first heating cycle, (b) block with additional lateral thermal insulation prior to further testing, (c) block during heating.

temperatures, the helium atmosphere was replaced every two days as the cooling rate gradually increased. In total, 205 heating and cooling cycles were performed. Each cycle required continuous monitoring of the inductor parameters and precise control of the water flow rate.

Temperature monitoring was carried out using five thermocouples. The positions of thermocouples T1–T4 are shown in Fig. 13a, while an additional thermocouple (Tw) measured the temperature of the cooling water at the outlet. The inlet water temperature remained stable between 14 and 17°C. A representative temperature evolution during one day of thermal cycling is shown in Fig. 13b. The inductor power was adjusted such that the temperature at the outer edge of the hexagonal block (T3) increased from approximately 360°C to 920°C within less than 2000 s. Fig. 13c compares a typical heating and cooling cycle with the simulated temperature profile shown in Fig. 2b. Overall, the total duration of the thermal cycle achievable with the present experimental setup is similar to that assumed in the simulated DEMO pulse. However, differences in the transient behavior are evident. In the initial stage of heating, the temperature increase is slower than in the simulated conditions, followed by a period of more rapid heating, resulting in a slightly shorter effective heating phase. In contrast, the cooling stage is significantly slower than predicted by the simulation. These deviations indicate that, while the current setup allows reproduction of the overall temperature range and cycle duration, further modifications of the experimental facility, particularly aimed at enhancing the cooling efficiency, are required to more closely match the thermal transients expected under reactor-relevant conditions.

The temperature measured on the outer flat surface (T1) was consistently slightly lower than that at the outer edge (T3), with differences of 30–50°C depending on temperature. The temperature difference between the interior of the block (T4) and the outer surface did not exceed 70°C at the end of the heating stage and 110°C at the end of the cooling stage. These results indicate that segmentation of the block leads to significantly more uniform induction heating compared with the one-piece configuration.

A simplified order-of-magnitude estimate of thermally induced stresses can be made using $\sigma_{th} \approx E\alpha\Delta T$. Using $E = 295$ GPa and $\alpha = 7.6–8.8 \times 10^{-6}$ $K^{-1}$ for $TiBe_{12}$ [2,14], temperature differences of 70–110°C measured in the segmented block correspond to estimated thermal stresses on the order of 150–300 MPa. For the one-piece block, such an estimate cannot be made directly because the temperature on the inner surface of the block wall was not measured during the first and only heating cycle. Nevertheless, considering the estimated electromagnetic penetration depth of approximately 4.5 mm at 2400 Hz and the minimum wall thickness of about 22.5 mm, it can be assumed that significantly larger temperature gradients were generated in the one-piece configuration. If a conservative characteristic temperature difference of approximately 300°C is assumed, the corresponding thermal stresses may approach values on the order of 700–900 MPa. The compressive strength of $TiBe_{12}$ is reported to be approximately 2000 MPa [8,10], whereas the tensile and bending strengths of brittle intermetallic materials are typically significantly lower, potentially by nearly one order of magnitude. Therefore, localized tensile stresses generated

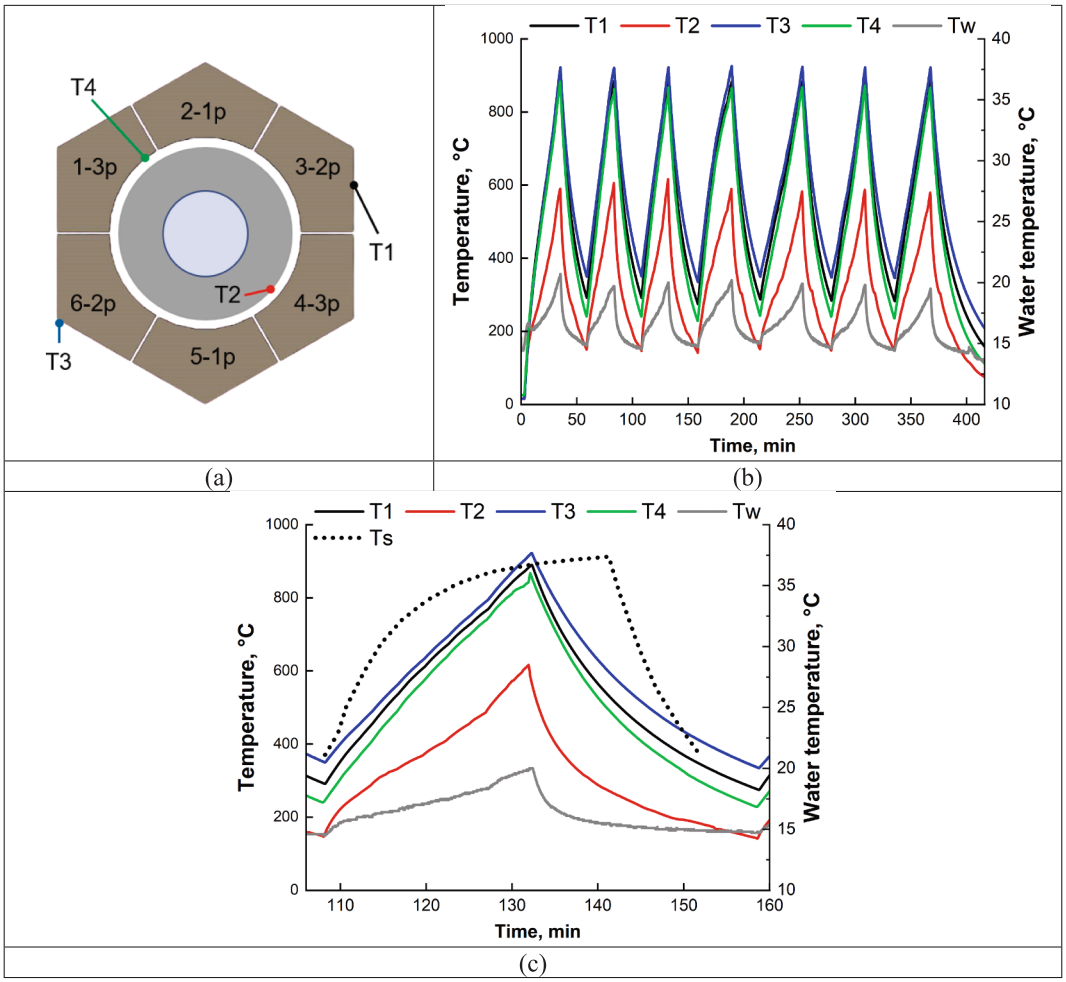


**Fig. 13.** Temperature monitoring during thermal cycling of the segmented $TiBe_{12}$ block: (a) locations of thermocouples T1–T4, (b) representative temperature evolution during one day of thermal cycling, (c) enlarged view of a single heating and cooling cycle compared with the simulated temperature profile from Fig. 2b.

during non-uniform induction heating could exceed the effective fracture strength of the material and promote crack initiation during the first heating cycle.

Although the minimum wall thickness remained similar in both the one-piece and segmented configurations, segmentation substantially altered the electromagnetic and thermal conditions during induction heating. In the one-piece block, the closed-loop geometry promoted concentration of induced currents along the outer perimeter, so that only a limited near-surface region was directly heated by induced currents, while the inner part of the wall was heated mainly by thermal conduction. In contrast, each segmented element formed a smaller independent current path and was exposed to induction heating from several free surfaces. As a result, the ratio of directly heated near-surface volume to the total segment volume increased, leading to a significantly more homogeneous temperature distribution and lower thermal stresses. Based on these considerations, it was assumed that the fracture of the one-piece $TiBe_{12}$ block was primarily associated with localized induction heating and the resulting thermal stress concentration, which motivated the transition to the segmented block design.

Fig. 14a,b shows the condition of the $TiBe_{12}$ segments after 17 and 60 thermal cycling cycles, respectively. In both cases, visual inspection confirmed that the segments retained their integrity, and no cracks or macroscopic defects were observed. After 114 cycles, complete disassembly revealed that all segments were still intact and free of cracks (Fig. 14c). However, minor chipping of small material pieces was observed at the outer edges of some segments (Fig. 14d). This effect is most likely associated with localized overheating caused by induced currents and occasional sparking at the interfaces between the $TiBe_{12}$ segments and the nickel–chromium wire used for mechanical fixation. After reaching 202 thermal cycles, the block was inspected again without full disassembly. All segments remained intact, and no surface cracks were detected. Overall, the results demonstrate that segmentation of the $TiBe_{12}$ block effectively suppresses crack formation during thermal cycling under induction heating by reducing temperature gradients and associated thermal stresses.

*Additional thermal cycling experiments*

After 202 thermal cycles, additional experiments were performed in order to further characterize the thermal behavior of the segmented $TiBe_{12}$ block and to assess the capabilities and limitations of the experimental setup under enhanced heating and cooling conditions. In particular, an approximate evaluation of the heating power delivered to the block was carried out. The heating power was estimated based on a thermal balance between the heat transferred to the cooling water and the measured temperature difference between the inlet and outlet of the stainless-steel pressure tube at a known water mass flow rate. Heat losses from the top and side surfaces of the block, as well as from the pressure tube, were not taken into account. To reduce these losses, the block was covered with thermal insulation on the top and lateral surfaces. Consequently, the obtained values represent the power transferred to the cooling water and thus provide a lower-bound estimate of the effective induction heating power of the $TiBe_{12}$ block.

The locations of thermocouples T1–T4 used for temperature

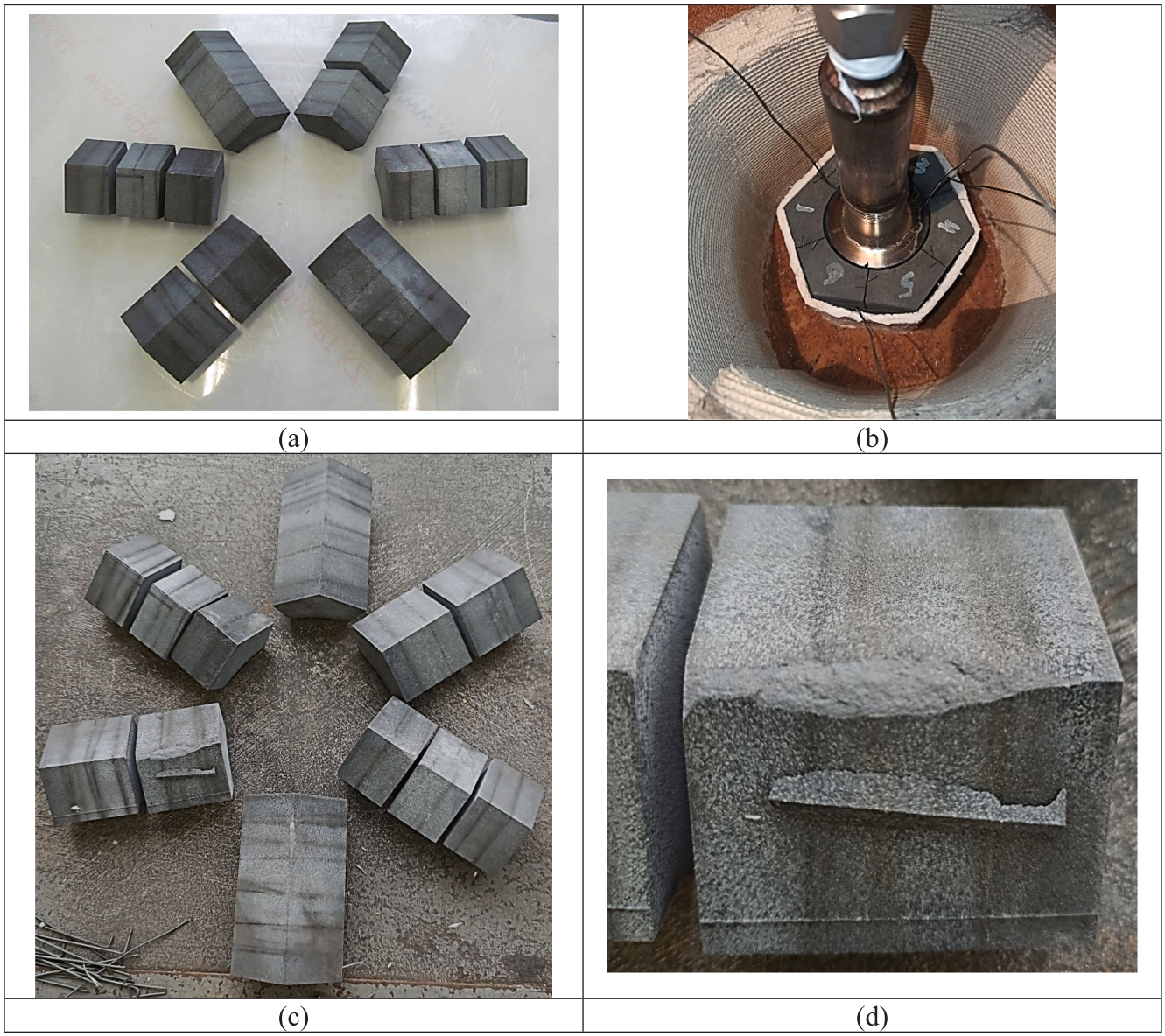


**Fig. 14.** Condition of the segmented $TiBe_{12}$ block after different numbers of thermal cycles: (a) $TiBe_{12}$ segments after complete disassembly following 17 heating and cooling cycles, (b) segmented block after partial disassembly following 60 cycles, (c, d) segmented block after 114 cycles, including enlarged views highlighting minor chipping at the segment corners.

monitoring are shown in Fig. 15a. The evolution of temperatures at the control points, together with the outlet water temperature and the corresponding estimated heating power, is presented in Fig. 15b. At the minimum inductor power, a steady-state temperature of approximately 420°C was recorded by thermocouple T1, corresponding to a water heating power of about 2.6 kW. With increasing inductor power, steady-state temperatures of approximately 650°C and 920°C were achieved at T1, corresponding to water heating powers of about 4.0 kW and 6.8 kW, respectively. During these measurements, thermocouple T3 was found to be displaced and to indicate the surface temperature of the steel pressure tube rather than the inner surface of the composed block.

Immediately after the power evaluation experiments, the block was subjected to additional heating at the maximum available inductor power in order to increase insufficient heating rates. In this mode, the block was heated from approximately 350°C to peak temperatures of 1000°C and 1100°C. The corresponding temperature evolution is shown in Fig. 15c. Under these conditions, the estimated power transferred to the cooling water reached values of approximately 10–11 kW. The maximum heating rates were 1.1–1.2 K/s, significantly exceeding the heating rate assumed in the simulated DEMO pulse (0.8 K/s), whereas the cooling rates remained substantially lower than those predicted by the simulation.

The cooling rates achieved during thermal cycling of the segmented $TiBe_{12}$ block remained noticeably lower than those assumed in the simulated DEMO pulse. This limitation is primarily associated with the cooling conditions available in the present experimental setup. In the DEMO HCPB blanket, heat removal is expected to occur through high-pressure high-velocity helium flow, which can provide significantly more intensive cooling of the multiplier blocks. Such cooling conditions could not be reproduced in the present facility. At the same time, cooling in the blanket remains inherently surface-dominated because heat extraction occurs through the interfaces between the $TiBe_{12}$ blocks and the surrounding cooled structures. Therefore, although the achievable cooling intensity was lower than under DEMO-relevant conditions, the qualitative nature of the cooling process remains relevant for studying thermally induced stress development in $TiBe_{12}$ blocks.

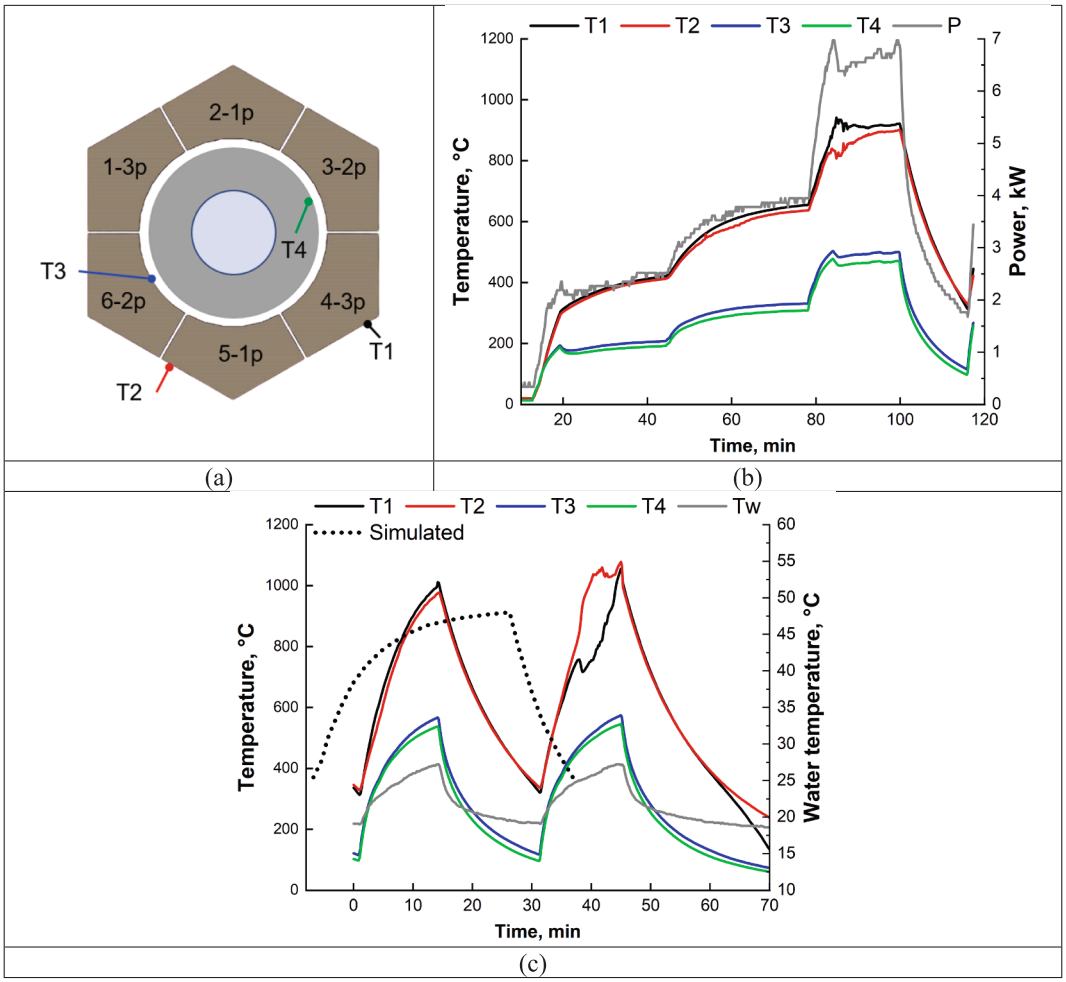


**Fig. 15.** Evaluation of heating power during thermal cycling of the segmented $TiBe_{12}$ block: (a) locations of thermocouples T1–T4, (b) temperature evolution of thermocouples T1–T4, outlet water temperature Tw, and corresponding estimated heating power, (c) temperature evolution during heating to 1000–1100°C at maximum inductor power compared with the simulated pulse from Fig. 2b.

To further investigate the cooling capability of the setup and to simulate potential displacement of blanket components, an additional experiment was performed in which two $TiBe_{12}$ segments with a height of 100 mm were placed in direct contact with the water-cooled stainless-steel pressure tube, positioned opposite each other. The experimental configuration during heating is shown in Fig. 16a. Two thermal cycles were conducted: a gradual heating cycle followed by a cycle at maximum inductor power. The corresponding temperature evolution is presented in Fig. 16b.

Even under these conditions, the maximum temperature on the segment surfaces did not exceed approximately 770°C, while the temperature at the $TiBe_{12}$ / steel interface reached about 530°C, resulting in a temperature gradient of up to 220°C across the segment thickness. The maximum heating rate of the segment outer surface reached 1.3 K/s, exceeding the simulated value, whereas the maximum cooling rate remained limited to about 1.2 K/s, still lower than the simulated cooling rate of 1.33 K/s. The total cooling time from 770°C to 370°C was approximately 700 s, compared with about 500 s in the simulation. These results indicate that even direct contact with the water-cooled steel pressure tube does not provide sufficiently rapid cooling to fully reproduce the simulated thermal transients. At the same time, the experimentally obtained temperature gradients and heating and cooling rates provide valuable reference data for the validation and refinement of thermo-mechanical simulations. The observed discrepancies between experimental and simulated cooling behavior suggest that further optimization of the cooling configuration or revision of the assumed boundary conditions may be required in order to achieve closer correspondence with reactor-relevant thermal transients.

After completion of all experiments, corresponding to a total of 205 heating and cooling cycles (including three additional cycles for power assessment and high-temperature heating), the $TiBe_{12}$ segments were fully disassembled and inspected (Fig. 17). All segments retained their structural integrity, and no cracks were observed. Minor chipping of small material pieces was detected at the outer edges and corners of some segments, particularly in regions exposed to electrical contact with the nickel–chromium fixation wire and the BrB2 spacer rods (Fig. 17a). These effects are attributed to localized overheating and occasional sparking associated with induced currents. In contrast, the surfaces facing the stainless-steel pressure tube remained unchanged (Fig. 17b). Segments with a height of 100 mm did not exhibit cracking, indicating that further reduction of block height is unlikely to provide additional benefit in reducing thermal stresses during thermal cycling. A detailed microstructural characterization of the $TiBe_{12}$ segments will be performed in subsequent work to clarify the mechanisms responsible for the observed surface chipping and to quantify the effect of thermal cycling on the microstructure and mechanical properties. The obtained results will contribute to the validation of thermo-mechanical material properties and numerical models relevant for fusion blanket applications.

## Conclusions

Thermal cycling experiments were conducted on titanium beryllide

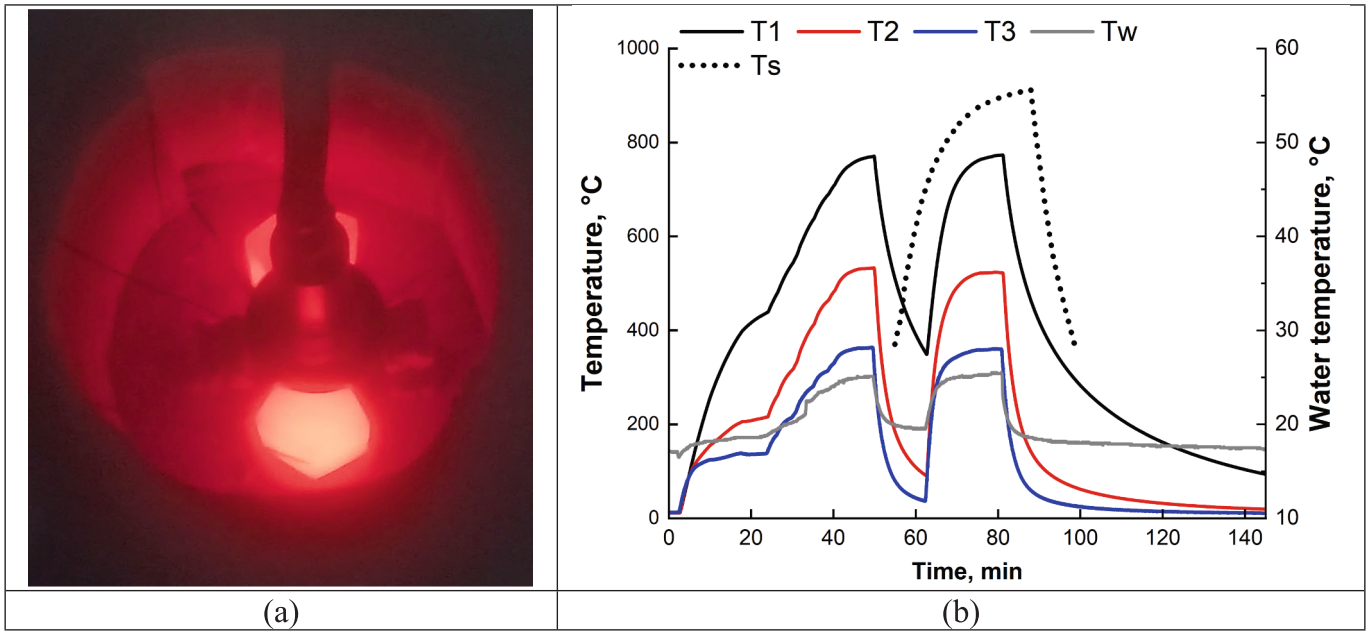


**Fig. 16.** Thermal cycling of two $TiBe_{12}$ segments (100 mm height) in direct contact with the stainless-steel pressure tube: (a) experimental assembly during heating, (b) temperature evolution, where T1 is the segment outer surface temperature, T2 the temperature at the $TiBe_{12}$–steel interface, T3 the temperature of the free surface of the steel tube, Tw the outlet water temperature, and Ts the simulated temperature profile from Fig. 2b.

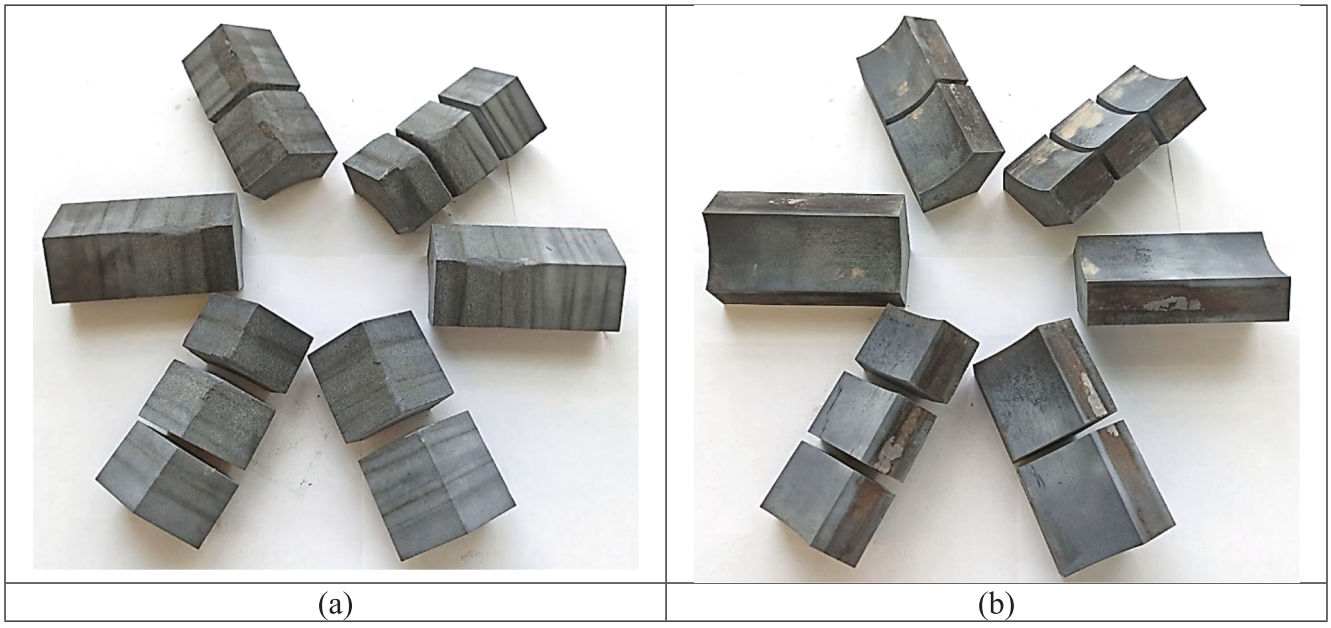


**Fig. 17.** $TiBe_{12}$ segments after 205 heating and cooling cycles: (a) outer segment surface, (b) segment surface facing the stainless-steel pressure tube.

($TiBe_{12}$) blocks using induction heating and water cooling to simulate transient thermal loading relevant to the DEMO HCPB blanket concept. Thermal cycling of a one-piece hexagonal $TiBe_{12}$ block resulted in fracture during the first heating cycle, which is attributed to strongly non-uniform heating caused by the closed-loop geometry of the solid block under induction heating and the resulting high thermal stresses near the outer surface. An alternative segmented block configuration was therefore investigated. The second hexagonal $TiBe_{12}$ block was subdivided into 12 segments, forming a composed block with reduced electrical and thermal continuity. This configuration enabled more uniform induction heating and effectively reduced thermal stresses. The segmented block successfully withstood 205 heating and cooling cycles without macroscopic cracking or fracture.

During thermal cycling, maximum surface temperatures of approximately 920–930°C and minimum temperatures between cycles of 350–370°C were achieved. Compared with the simulated DEMO pulse, heating occurred somewhat faster, whereas cooling was on average slower. Nevertheless, the achieved temperature range and cycle duration were sufficiently close to reactor-relevant conditions to provide meaningful insight into the thermal response of $TiBe_{12}$.

Additional experiments showed that $TiBe_{12}$ segments did not fracture at heating rates up to 1.1–1.3 K/s, even at maximum inductor power. Cooling rates of approximately 1.2 K/s, achieved with direct contact with a water-cooled stainless-steel pressure tube, also did not

induce cracking. These results indicate that $TiBe_{12}$ exhibits good resistance to rapid thermal transients provided that internal temperature gradients are limited.

Minor chipping of near-surface regions was observed at segment edges and corners after extended cycling, likely related to localized overheating and electrical sparking associated with experimental fixation elements rather than to bulk thermal loading. Such effects are not expected under reactor-relevant volumetric neutron heating. Overall, the results demonstrate that segmented $TiBe_{12}$ blocks can withstand cyclic exposure to temperatures between approximately 360 and 920°C for at least 205 cycles.

## CRediT authorship contribution statement

**Ramil Gaisin:** Writing – review & editing, Writing – original draft, Visualization, Methodology, Investigation. **Sergey Udartsev:** Writing – review & editing, Writing – original draft, Investigation. **Maxim Kolmakov:** Methodology, Investigation. **Vladimir Chakin:** Writing – review & editing, Writing – original draft, Supervision, Investigation. **Pavel Vladimirov:** Writing – review & editing, Writing – original draft, Supervision, Methodology. **Francisco A. Hernández:** Writing – review & editing, Supervision, Funding acquisition, Conceptualization.

## Declaration of competing interest

The authors declare that they have no known competing financial interests or personal relationships that could have appeared to influence the work reported in this paper.

## Acknowledgements

This work has been carried out within the framework of the EUROfusion Consortium, funded by the European Union via the Euratom Research and Training Programme (Grant Agreement No 101052200 — EUROfusion). Views and opinions expressed are however those of the author(s) only and do not necessarily reflect those of the European Union or the European Commission. Neither the European Union nor the European Commission can be held responsible for them.

## Data availability

Data will be made available on request.

## References

[1] F.A. Hernández, P. Pereslavtsev, G. Zhou, B. Kiss, Q. Kang, H. Neuberger, V. Chakin, R. Gaisin, P. Vladimirov, L.V. Boccaccini, G.A. Spagnuolo, S. D'Amico, I. Moscato, Advancements in the helium-cooled pebble bed breeding blanket for the EU DEMO: holistic design approach and lessons learned, Fusion Sci. Technol. 75 (2019) 352–364, https://doi.org/10.1080/15361055.2019.1607695.

[2] R. Gaisin, V. Chakin, P. Vladimirov, F.A. Hernández, S. Udartsev, A. Vechkutov, M. Kolmakov, Industrial-scale manufacturing experience of titanium beryllide block for DEMO blanket application, Fusion Eng. Des. 161 (2020) 111862, https://doi.org/10.1016/j.fusengdes.2020.111862.

[3] R. Gaisin, Y. Frants, M. Kolmakov, B. Zorin, M. Kylyshkanov, M. Podoinikov, S. Udartsev, A. Vechkutov, V. Chakin, P. Vladimirov, Beryllium intermetallics: industrial experience on development and manufacture, Nucl. Mater. Energy 35 (2023) 101444, https://doi.org/10.1016/j.nme.2023.101444.

[4] Ye. Frants, A. Borsuk, A. Vechkutov, K. Zenkov, B. Zorin, M. Kylyshkanov, M. Podoinikov, S. Udartsev, P. Vladimirov, R. Gaisin, Titanium beryllide as an alternative to beryllium in nuclear and thermonuclear engineering, capabilities of UMP JSC in the technology development and beryllides products manufacture, in: J. Phys. Conf. Ser., IOP Publishing Ltd, 2022. Doi: 10.1088/1742-6596/2155/1/012015.

[5] K. Tsuchiya, T. Hoshino, H. Kawamura, Y. Mishima, N. Yoshida, T. Terai, S. Tanaka, K. Munakata, S. Kato, M. Uchida, M. Nakamichi, H. Yamada, D. Yamaki, K. Hayashi, Development of advanced tritium breeders and neutron multipliers for DEMO solid breeder blankets, Nucl. Fusion 47 (2007) 1300, https://doi.org/10.1088/0029-5515/47/9/029.

[6] V. Chakin, A. Fedorov, R. Gaisin, M. Zmitko, Swelling of highly neutron irradiated beryllium and titanium beryllide, Journal of Nuclear Engineering 3 (2022) 398408, https://doi.org/10.3390/jne3040026.

[7] V. Chakin, R. Rolli, R. Gaisin, U. Hoeppener-Kramar, M. Nakamichi, M. Zmitko, Tritium release and retention in beryllium and titanium beryllide after neutron irradiation up to damage doses of 23-38 dpa, Fusion Eng. Des. 161 (2020) 111938, https://doi.org/10.1016/j.fusengdes.2020.111938.

[8] R. Gaisin, R. Rolli, M. Podoinikov, V. Kuksenko, K. Seemann, T. Bergfeldt, V. Chakin, P. Vladimirov, Microstructure and high-temperature mechanical performance of industrial-scale titanium and chromium beryllides for fusion applications, J. Alloy. Compd. 1044 (2025) 184503, https://doi.org/10.1016/j.jallcom.2025.184503.

[9] J.-H. Kim, T. Hwang, Y. Sugimoto, M. Nakamichi, M. Miyamoto, Deuterium retention properties of vanadium beryllide (Be12V) for advanced neutron multiplier applications, Fusion Eng. Des. 201 (2024) 114278, https://doi.org/10.1016/j.fusengdes.2024.114278.

[10] T. Hwang, J.-H. Kim, Y. Akatsu, Y. Sugimoto, S. Nakano, M. Nakamichi, Compression properties of beryllide pebbles at high temperatures, Fusion Eng. Des. 194 (2023) 113844, https://doi.org/10.1016/j.fusengdes.2023.113844.

[11] K.A. Walsh, Beryllium chemistry and processing, ASM International (2009).

[12] R. Gaisin, V. Chakin, R. Rolli, J. Hoffmann, H. Leiste, T. Bergfeldt, U. Jäntsch, M. Klimenkov, J. Lorenz, A. Goraieb, P. Vladimirov, A. Möslang, Synthesis of Be12Ti compound via arc melting or hot isostatic pressing, J. Alloy. Compd. 818 (2020) 152919, https://doi.org/10.1016/j.jallcom.2019.152919.

[13] R. Gaisin, V. Chakin, M. Duerrschnabel, R. Rolli, T. Weingaertner, A. Goraieb, P. Vladimirov, Effect of HIP at 800 and 900 °C on microstructure and properties of extruded Be-Ti composites, Nucl. Mater. Energy 24 (2020) 100771, https://doi.org/10.1016/j.nme.2020.100771.

[14] R. Gaisin, V. Kuksenko, M. Duerrschnabel, V. Chakin, A. Goraieb, P. Vladimirov, Effect of HIP at 1000–1200 °C on microstructure and properties of extruded Be-Ti composites, Nucl. Mater. Energy 30 (2022) 101128, https://doi.org/10.1016/j.nme.2022.101128.

[15] T. Hwang, J.-H. Kim, S. Nakano, M. Nakamichi, Mechanical properties of beryllium-titanium intermetallic compounds fabricated by plasma sintering, Nucl. Mater. Energy 30 (2022) 101117, https://doi.org/10.1016/j.nme.2022.101117.

[16] S. D'Amico, P.A. Di Maio, X.Z. Jin, F.A. Hernández Gonzalez, I. Moscato, G. Zhou, Preliminary thermal-hydraulic analysis of the EU-DEMO Helium-Cooled Pebble Bed fusion reactor by using the RELAP5-3D system code, Fusion Eng. Design 162 (2021) 112111, https://doi.org/10.1016/j.fusengdes.2020.112111.

[17] V. Rudnev, D. Loveless, R.L. Cook, Handbook of Induction Heating, 2nd ed., CRC Press, Boca Raton, 2017. Doi: 10.1201/9781315117485.